

Linköping Studies in Science and Technology
Licentiate Thesis No. 1537

HiPIMS-based Novel Deposition Processes for Thin Films

Asim Aijaz



Linköping University
INSTITUTE OF TECHNOLOGY

LIU-TEK-LIC-2012:22
Plasma & Coatings Physics Division
Department of Physics, Chemistry and Biology (IFM)
Linköping University
SE-581 83 Linköping, Sweden

© Asim Aijaz 2012

ISBN: 978-91-7519-870-5

ISSN 0280-7971

Printed by LiU-tryck
Linköping, Sweden, 2012

Abstract

In this research, high power impulse magnetron sputtering (HiPIMS) based new deposition processes are introduced to address; the issue of low degree of ionization of C in magnetron sputtering discharges, and the difficulty encountered in thin film deposition on complex-shaped surfaces. The issue of low degree of C ionization is addressed by introducing a new strategy which is based on promoting the electron impact ionization of C by increasing the electron temperature in the plasma discharge using Ne, instead of conventionally used Ar. The Ne-based HiPIMS process provides highly ionized C fluxes which are essential for the synthesis of high-density and sp^3 rich amorphous carbon (a-C) thin films such as diamond-like carbon (DLC) and tetrahedral a-C (ta-C). The feasibility of coating complex-shaped surfaces is demonstrated by using the dual-magnetron approach in an open-field (magnetic field of the magnetrons) configuration and performing sideways deposition of Ti films. The HiPIMS-based open-field configuration process enhances the sideways transport of the sputtered flux — an effect which is observed in the case of HiPIMS.

The characterization of the Ne-HiPIMS discharge using a Langmuir probe and mass spectrometry shows that it provides an increase in the electron temperature resulting in an order of magnitude decrease in the mean ionization length of the sputtered C as compared to the conventional Ar-HiPIMS discharge. The C^{1+} ion energy distribution functions exhibit the presence of an energetic C^{1+} ion population and a substantial increase in the total C^{1+} ion flux. The higher C^{1+} ion flux facilitates the growth of sp^3 rich carbon films with mass densities, measured by x-ray reflectometry, reaching as high as approx. 2.8 gcm^{-3} .

The dual-magnetron open-field configuration process is operated in DCMS as well as in HiPIMS modes. The plasma characterization, performed by Langmuir probe measurements and optical emission spectroscopy, shows that the plasma density in the Ti-HiPIMS discharge is higher than that of the Ti-DCMS discharge. This results in the higher ionized fraction of the sputtered Ti in the case of HiPIMS. The film uniformity and the deposition rate of the film growth, obtained by employing scanning electron microscopy, demonstrate that the sideways deposition approach can be used for depositing thin films on complex-shaped surfaces.

Preface

This Licentiate Thesis is a part of my PhD studies in the Plasma and Coatings Physics Division at Linköping University. The goal of my doctorate project is to develop new magnetron sputtering based processes which facilitate the synthesis of DLC and ta-C at laboratory as well as at industrial scale. The research is financially supported by the Swedish Research Council (VR) through the contracts 621-2008-3222 and 621-2011-4280.

Appended Papers

1. **A strategy for increased carbon ionization in magnetron sputtering discharges**

Asim Aijaz, Kostas Sarakinos, Daniel Lundin, Nils Brenning and Ulf Helmersson

Diamond & Related Materials, **23** (2012) 1.

2. **Dual-magnetron open field sputtering system for sideways deposition of thin films**

Asim Aijaz, Daniel Lundin, Petter Larsson and Ulf Helmersson

Surface & Coatings Technology, **204** (2010) 2165.

Publications not included in the thesis

- 1. Patent: Sputtering process**
Ulf Helmersson, Nils Brenning and **Asim Aijaz**

Patent application (Approved) 2012.
- 2. A novel high-power pulse PECVD method**
Henrik Pedersen, Petter Larsson, **Asim Aijaz**, Jens Jensen and Daniel Lundin

Accepted for publication in Surface & Coatings Technology, 2012.
- 3. Effect of peak power in reactive high power impulse magnetron sputtering of titanium dioxide**
Montri Aiempanakit, Ulf Helmersson, **Asim Aijaz**, Petter Larsson, Roger Magnusson, Jens Jensen and Tomáš Kubart

Surface & Coating Technology, 205 (2011) 4828.
- 4. Understanding the discharge current behavior in reactive high power impulse magnetron sputtering**
Montri Aiempanakit, **Asim Aijaz**, Daniel Lundin, Ulf Helmersson and Tomáš Kubart

In manuscript.
- 5. Deposition of yttria stabilized zirconia thin films for solid oxide fuel cells by high power impulse magnetron sputtering and pulsed magnetron sputtering**
Steffen Søndersby, **Asim Aijaz**, Kostas Sarakinos, Ulf Helmersson and Per Eklund

In manuscript.

Acknowledgements

First of all, I would like to thank **Almighty Allah**, Who is the real source of knowledge and wisdom.

Furthermore, there are a number of people whose valuable contributions made this journey rewarding for me. I would like to extend my deepest gratitude towards them. These are:

Ulf Helmersson, my main-supervisor, who gave me the opportunity to conduct this research and whose guidance, patience, encouragement and difficult questions, helped me to progress.

Kostas Sarakinos, my co-supervisor, whose passion and dedication for science is inspirational. I like to thank him for his support, encouragement, time and for guiding me to new directions in my research.

Daniel Lundin, for being supportive and encouraging co-worker, for providing great insights into the subject and for always showing the positive aspects of even the *disappointing-looking* outcomes.

All other members of the Plasma and Coatings Physics division, for creating an atmosphere of quality research together with fun. Friends and colleagues in the **Thin Film Physics** and **Nanostructured Materials** divisions. You all contributed in one way or the other.

My friends in Sweden and back in Pakistan, each of them is equally valuable for me.

All my family members, without their sacrifices, encouragement, support and prayers, I am nothing!

My soul mate, my wife, **Yasra**, who always brings sense of friendship and support to me. In every moment that I spend with You, I live a life!

My **Mother**; the person behind all my success, the source of inspiration at all stages of my life, my reason to smile and whose contribution to my life can not be described in words.

Contents

Abstract	I
Preface	III
Acknowledgements	V
Appended Papers	VII
Publications not included in the thesis	VIII
1 Introduction	1
1.1 Background and Motivation	1
1.2 Goals and Research Strategy	4
1.3 Outline	4
2 Plasma-Assisted Physical Vapor Deposition	5
2.1 Sputtering	5
2.2 Magnetron Sputtering	7
2.2.1 Direct current magnetron sputtering (DCMS)	8
2.2.2 High power impulse magnetron sputtering (HiPIMS)	8
3 Basic Plasma Physics	11
3.1 Introduction	11
3.2 Plasma for Material Synthesis	12
3.3 Ionization Processes	16
4 Amorphous Carbon Growth	21
4.1 Introduction	21
4.2 Different Forms of Amorphous Carbon	22
4.3 The Densification Model	22

5	Amorphous Carbon Growth and Ionized PVD	27
5.1	Filtered Cathodic Vacuum Arc (FCVA)	27
5.2	Pulsed Laser Deposition (PLD)	28
5.3	HiPIMS	29
6	Research Strategy and Experimental Details	31
6.1	Research Strategy	31
6.2	Plasma Characterization	32
6.2.1	Langmuir Probe Measurements	33
6.2.2	Mass Spectrometry	36
6.2.3	Optical Emission Spectroscopy	38
6.3	Film Characterization	40
6.3.1	X-ray Reflectometry	40
6.3.2	Scanning Electron Microscopy	42
7	Summary of the Appended Papers	43
8	Ongoing Work and Future Outlook	45
9	References	47
	Paper 1-2	51

1. Introduction

1.1 Background and Motivation

Thin films are structures with thicknesses ranging from several nanometers up to several micrometers that are formed when atomic layers of a material are deposited on a surface to alter its properties and functionality [1]. The desired properties can be achieved by mono-elemental films (such as Au thin films are used as corrosion-resistant electrically conductive layers in electronic industry) [2] or films that consist of more than one elements (such as Al_2O_3 films are used as protective coatings for cemented carbide cutting tools) [3]. The ultimate goal of thin film science and technology is to develop tailor-made materials in such a way that they exhibit different attributes and hence they can be used in various applications. An example is amorphous carbon (a-C) films, which exhibit unique and adjustable properties ranging from those of graphite to those of diamond — finding their applications ranging from lubrication to ultra-dense hard coatings [4,5]. These properties are controlled by the hybridization state of the carbon atoms i.e. the ratio of the sp^3 to sp^2 hybridized bonds and the atomic H content [5]. On the basis of the atomic H content, a-C can be classified as H-free amorphous carbon (a-C) as well as hydrogenated amorphous carbon (a-C:H) [4,5]. Apart from H, the material can also adopt a large number of stable forms by bonding strongly to other atoms such as Si, N, B and F which leads to a wide range of carbon-based thin films and coatings [4]. Amorphous carbon-metal nanocomposites are another emerging material systems where metal atoms are incorporated into a-C matrix to tailor, for example, the electrical properties [6]. Examples of such materials are TiC and CrC [6]. Some noble metals such Ag, which are weak carbide formers, are also incorporated into a-C and they have emerged as a promising addition in antibacterial, optical and tribological applications [7].

Amorphous carbon thin films for specific applications are nowadays commonly synthesized by chemical vapor deposition (CVD) — where a vapor of the depositing carbon is created using chemical reaction of gases [5,8] — and physical vapor deposition (PVD), where the same is achieved through physical processes such as sputtering or evaporation from a graphite solid source (referred to as target) [5]. Both of these groups of methods are widely used for a-C synthesis at laboratory as well as at industrial scale. The-state-of-the-art approaches for the synthesis of a-C using PVD methods include; cathodic arc evaporation (CVA), pulsed laser deposition (PLD) as well as magnetron sputtering based methods, e.g. radio frequency magnetron sputtering (RFMS) [5,9]. CVA, PLD and RFMS are also termed as plasma-assisted PVD methods since in these methods, the vapor generation and transport to the substrate involve an assistance of plasma. The plasma for material synthesis is described in chapter 2.

In a plasma-assisted PVD method, the sp^3/sp^2 ratio — vital for the a-C film functionality — can be controlled by the energy and the flux of the depositing species (carbon as well as the buffer gas species) [5,10]. The control over the energy becomes much easier if a large fraction of the depositing flux is ionized. In this case the energy of the depositing flux can be tuned by the use of an electric field, e.g. by applying a bias potential to the substrate (the place where the source material is deposited). Another important consideration with respect to the deposition of thin films (including a-C) is the geometry of the substrate. Often, the complex-shaped surfaces are encountered — e.g. engine valves covered by carbon-based wear-resistant coatings [11] — which makes it difficult to achieve uniformity in the coatings [12]. This difficulty can also be overcome by achieving highly ionized depositing fluxes, since electric and magnetic fields can also facilitate control over the direction of the ionized depositing flux [13,14].

The plasma-assisted PVD methods where more than 50% of the depositing material is ionized are called ionized PVD methods [15]. Both, CVA and PLD fall into this category since the ionized fraction of the depositing flux reaching up to 100% can be obtained using these methods thereby making the synthesis of dense and sp^3 rich a-C thin films possible [5]. However, they exhibit some drawbacks such as macroparticle ejection from

the target, lack of lateral film uniformity and in some cases, are difficult to scale-up [16,17]. Magnetron sputtering-based methods overcome the drawbacks which are inherent to CVA and PLD and therefore, these methods are technologically more relevant. However, highly ionized depositing fluxes cannot be created using conventional magnetron sputtering methods, such as direct current magnetron sputtering (DCMS) and RFMS [15]. For the case of a-C growth, this means that tailoring the properties of a-C thin films as well as the synthesis of dense and sp^3 rich a-C using these methods is difficult [5,9].

An emerging magnetron sputtering based technique is high power impulse magnetron sputtering (HiPIMS) [11,18]. HiPIMS provides a substantially higher ionization of the depositing flux as compared to the conventional magnetron sputtering methods. HiPIMS has already demonstrated its potential as an ionized PVD method for most commonly used metals such as Cu, Ti, Ta, Al etc [15]. For example, an ionized fraction of more than 90% has been reported for Ti using HiPIMS [19]. The potential of HiPIMS for non-metals such as C, has not been fully explored and a limited research has been carried out for the synthesis of a-C using HiPIMS. In one report, DeKoven *et al.* showed that an ionized fraction of only 5% is achieved in C-HiPIMS discharges [20]. In another study by Sarakinos *et al.*, it has been shown that using HiPIMS, the a-C films with mass densities reaching up to 2.2 gcm^{-3} and an sp^3 fraction of 45% can be grown [21]. Moreover, the same study reported that the implementation of HiPIMS affects mainly the ionization of the buffer gas (Ar) atoms while the C ionization degree remains at the same levels as those achieved by the conventional DCMS processes. These results show that there is much room for the improvement in the conventional HiPIMS-based C discharges as well as there is a need for understanding and addressing the fundamental issue of low degree of C ionization in magnetron sputtering discharges. By addressing this issue, an industrially more relevant technique will be available for the synthesis of dense and sp^3 a-C as well as it will facilitate the deposition of a-C coatings on complex-shaped surfaces.

1.2 Goals and Research Strategy

The first goal of this research is to understand and address the issue of low degree of carbon ionization in magnetron sputtering discharges — by using HiPIMS as the model magnetron sputtering based process — and grow high density and sp^3 rich a-C coatings. The goal is achieved by introducing a new strategy for increasing carbon ionization which leads to developing a new HiPIMS-based process. The strategy is based on increasing the electron temperature in the plasma discharge by using Ne as the sputtering gas, instead of conventionally used Ar. Both, the Ne-HiPIMS and Ar-HiPIMS discharges are operated under the identical process conditions and plasma characterization is performed to compare the resulting plasma properties. Carbon thin films are synthesized under various deposition conditions and the resulting film properties are also compared.

The second goal is to develop a HiPIMS-based process for the synthesis of thin films on complex-shaped surfaces to fully exploit the potential of the new HiPIMS process for real applications. This goal is achieved by using the dual-magnetron approach with an open-field configuration and performing sideways deposition of Ti films, when the magnetrons are operated synchronously in DCMS as well as in HiPIMS modes. Ti is chosen as a model system, owing to the higher degree of ionization of Ti, achieved in magnetron sputtering discharges, as compared to C. The plasma characterization is performed to investigate and compare the degree of ionization in the DCMS and HiPIMS processes. Film characterization is performed to investigate the growth rate and the uniformity of the coatings.

1.3 Outline

The outline of this thesis is as follows: First, an overview of the sputtering-based methods is presented which is followed by a chapter on the basic plasma physics. After this, the fundamentals of a-C growth and state-of-the art of a-C growth are discussed. A chapter is included which describes in detail the research strategy and adopted methodology including experimental details — where the methods for plasma and film characterization are discussed. After this, the summary of the appended papers is presented and in the end, the thesis is concluded with the future outlook of the research work.

2. Plasma-Assisted Physical Vapor Deposition

As described in the previous chapter, there are various plasma-assisted PVD methods which are employed for the synthesis of thin films and coatings. Among these, the magnetron sputtering based methods are relevant to this work therefore, a brief description of commonly used magnetron sputtering based methods is provided in the following sections.

2.1 Sputtering

Sputtering is a physical process of ejecting the target atoms (source material) by means of an incident energy [1,22]. In a plasma based sputtering process, the incident energy is supplied via an interaction between the plasma constituents and the target atoms [22]. Sputtering plasma is the subject of the next chapter and here, a plasma can be considered simply as a collection of ions and electrons which is generated through an electrical discharge of an inert gas such as Ar [1]. Ions from the plasma are accelerated to the target by applying a negative potential to the target and as a result, various ion-solid surface interactions occur. These interactions can be influenced by many factors such as the incident ion energy, angles of incidence of the ions, binding energy of the target atoms, mass of the incident and target atoms etc., [22]. On the basis of the energy of the incident species, the process of sputtering is divided into three regimes of low ($< 1\text{keV}$), moderate ($1\text{-}50\text{ keV}$) and high energy ($>50\text{ keV}$), which are depicted in Figure 1 [22].

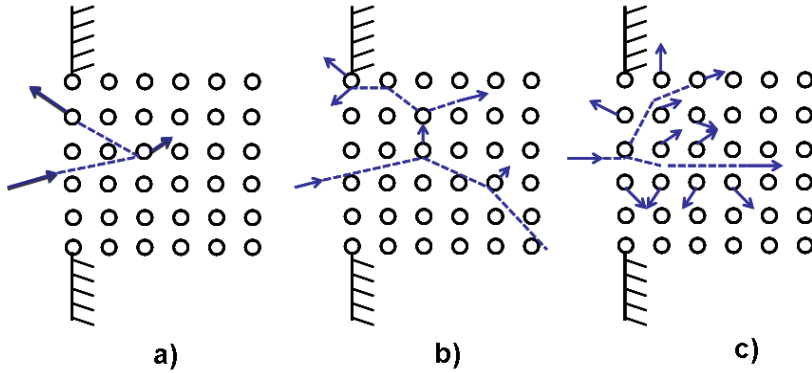


Figure 1. Energy regimes of sputtering: a) Single knock-on (low energy), b) Linear cascade (moderate energy) and c) Spike (high energy). (After P. Sigmund [22].)

In the low energy regime, the target atom which receives the incident energy at first place, through one-to-one interaction with the impinging ion, responds to it in an individual manner and therefore the process is referred to as the single-knock on [22]. In the moderate energy regime, the impinging atom can make a series of collisions with several target atoms thereby producing a cascade of ions along its path. The recoiled target atoms can be displaced from their sites in the solid and subsequently sputter out. This moderate energy regime is termed as the linear-cascade. In the high energy regime, the incident ion carries a substantially high energy which is enough to provide the binding energy to all atoms along its path. The condition of binary collisions (as is the case with the linear-cascade) no more holds and it is likely that the next atom which an incident atom interacts with, is already in motion. This regime is referred to as the spike [22].

The energies of the sputtered target atoms follow the Thomson distribution while they spread out according to cosine distribution [22]. The sputtered atoms traverse through the bulk plasma and thereby condense onto all surfaces in the reactor. Through their course, the sputtered atoms suffer elastic collisions with background gas atoms and are subsequently thermalized [22]. A fraction of them can also be ionized due to the inelastic collisions with electrons. How this ionization takes place will be discussed in connection to the plasma characteristics in chapter 3.

2.2 Magnetron Sputtering

In the process of plasma-based sputtering, the rate at which the target atoms are sputtered out is largely affected by the amount of inert gas ions that bombard the target surface. The supply of the inert gas ions can be increased by increasing the ionizing collisions of neutral gas atoms with the electrons. When this is achieved near the target surface, the sputtering efficiency increases dramatically [1,23]. This concept leads to the development of magnetron sputtering in which, the electrons in the plasma are confined in a region very close to the target surface using a magnetic field — by placing permanent magnets at the back of the target — thereby promoting the ionization [1,23]. The concept of a magnetron is illustrated in Figure 2.

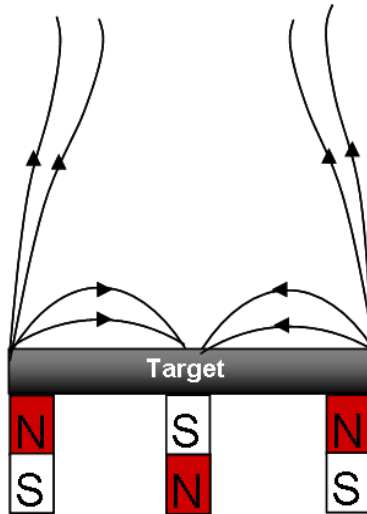


Figure 2. An schematic showing the principle of a magnetron. This is the cross-section of an unbalanced magnetron configuration.

The confined electrons will continuously create ions out of the inert gas which will subsequently bombard the target surface thereby increasing the rate of sputtering [1,23]. There are various methods in which the process of magnetron sputtering is realized. The commonly used among these are DCMS, RFMS [1,23] and HiPIMS [15]. DCMS and RFMS are the conventional magnetron sputtering methods while HiPIMS is one of the newly invented techniques. The research work presented in **paper I** and **paper II** was

carried out using DCMS and HiPIMS therefore, a brief description of only these two methods will be provided in the following section.

2.2.1 Direct Current Magnetron Sputtering

In DCMS, a constant power is applied to the target keeping the target power density in the order of a few Wcm^{-2} , which is necessary to prevent overheating of the target [15]. The discharge voltage is typically in the order of 300 V to 500 V and the resulting current densities are in the order of a few mAcm^{-2} [15]. This provides plasma densities in the order of $10^{14} - 10^{16} \text{ m}^{-3}$ [15]. This order of the plasma density results in low degree of ionization of a few percent of the sputtered material (less than 10% for metals) [15]. This means that the majority of the sputtered flux is neutral — with energy in the range between 5 – 10 eV [15]. DCMS discharges are therefore, not known to facilitate energetic deposition as well as achieving a control over the energy of the depositing flux in such a discharge is difficult.

2.2.2 High Power Impulse Magnetron Sputtering

In HiPIMS, the power to the cathode is applied in the form of short pulses (pulse on time between 5 – 5000 μs) such that the duty cycle is kept low (<5%). The pulse frequency in the range between 100 Hz to 10 kHz is used [15, 18]. The low duty cycle operation provides sufficient time for the target cooling. This also enables one to operate at peak powers in the order of several kWcm^{-2} [18].

A typical voltage-current characteristic from a HiPIMS discharge is presented in Figure 3, which shows that the discharge voltage in HiPIMS is twice as higher compared to those commonly used in DCMS discharges. The resulting target current densities in HiPIMS are in the order of several Acm^{-2} which are several orders of magnitude higher than those achieved in DCMS [15,18]. This in turn provides a discharge with plasma density in the order of $10^{18} - 10^{19} \text{ m}^{-3}$ [15,18]. It is mainly due to this high plasma density that with HiPIMS, a higher ionized fraction of the sputtered flux is obtained (about 90% for metals can be achieved) [19].

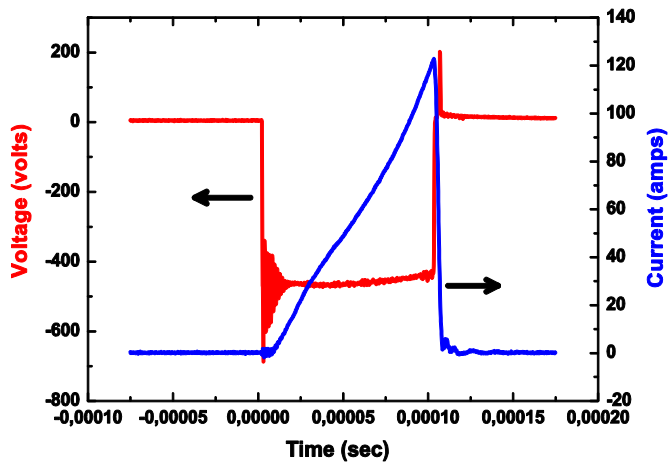


Figure 3. A HiPIMS voltage and current pulse recorded from a Ti discharge during the dual-magnetron open field sputtering process.

3. Basic Plasma Physics

3.1 Introduction

The term plasma was first coined by Irving Langmuir in 1928 and it describes a highly ionized state of matter which is collectively charge neutral (often termed as quasi-neutral) [24]. A plasma consists of ions, electrons and neutral atomic and molecular species and it exhibits a collective behavior in presence of external electric and magnetic fields. The bulk of the plasma contains almost equal amounts of negative and positive particles, i.e. ions and electrons ($n_i = n_e = n_0$) [24]. A plasma can be created by heating up a gas until the electrons from its freely moving atoms are released i.e. a gas breakdown occurs, to give a collection of randomly moving ions and electrons. The degree of ionization of the discharge gas commonly describes whether a plasma is weakly ionized or highly ionized [25].

Plasmas can also be classified as high temperature (hot) and low temperature (cold) plasmas [25]. Often a hot plasma is almost fully ionized, whereas a cold plasma may have ~1% gas ionization [25]. Examples of high temperature plasmas include fusion plasmas both inside stars as well as man-made in a reactor, and they are characterized by thermal equilibrium among their constituents. Gas discharge plasmas, such as those used in material synthesis, are usually regarded as low-temperature (and also low pressure) and non-thermal plasmas [25]. Ions, electrons and neutral atomic and molecular species in such plasmas are not in thermal equilibrium. Electrons being lighter and hence easily accelerated by external fields, possess high temperatures as compared to the other heavy plasma constituents [24]. For example, one often finds that neutral discharge gas is at room temperature, whereas the electrons reach several thousand degrees Kelvin. Through

momentum exchange collisions it is however possible to equalize the different temperatures. In such a way a thermal equilibrium among the plasma constituents can be attained by, for example increasing the discharge gas pressure, since it results in an increased amount of collisions [25].

3.2 Plasma for Material Synthesis

The plasma for material synthesis by PVD is usually created by means of an electrical discharge of an inert gas. This is achieved by introducing the inert gas (typically Ar) into the process chamber (see Figure 4), which is evacuated to a certain base pressure (the base pressure for the experiments performed in this research work was lower than 10^{-4} Pa while the working gas pressures from 0.66 Pa to 4.66 Pa were used). The process chamber is equipped with two electrodes acting as a cathode and an anode. Usually a negative potential is applied to the target material — which is mounted onto a magnetron in this work — to serve as the cathode while the walls of the chamber serve as the anode. The potential difference between the cathode and the anode will give rise to electric fields that can accelerate charged particles, which is crucial for transferring the neutral discharge gas to a plasma. The gas breakdown is initiated by an inelastic collision between a free electron (which might be present due to cosmic radiation or thermal energy) and a neutral gas atom — when the former is accelerated under the influence of the generated external electric field to an energy above the ionization energy of the neutral gas (about 15.76 eV in the case of Ar) [26]. In this way, the inelastic collisions give rise to the ionization as well as excitation of the gas atoms through the processes [26],



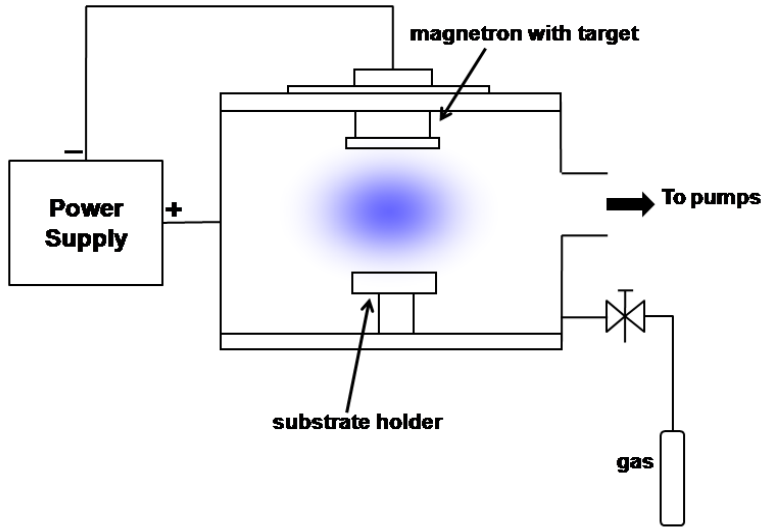


Figure 4. An schematic of a sputter deposition chamber. The target is clamped onto the magnetron which is mounted on the lid of the chamber. The target serves as the cathode while the chamber walls are made as the anode. An inert gas is let in through the leak valve and a plasma is created. The substrates for film deposition are placed on the substrate holder.

Each ionizing collision will result in two free electrons, which will also take part in the ionization of the gas atoms provided that they possess high enough kinetic energy. The ionized gas atoms, such as Ar^+ ions in this case, will be accelerated towards the negatively charged cathode and thereby ejecting the target atoms (through the process of sputtering, as described in chapter 2) along with the secondary electrons from the target surface. This process eventually results in a cascade of free electrons and ions, which finally leads to the gas breakdown. A continuous supply of the secondary electrons ensures that the enough Ar^+ ions are produced to generate again, during the process of sputtering, enough secondary electrons which can compensate for the loss of the charged particles through the diffusion to the walls. The overall result is a self-sustained plasma discharge. The de-excitations during the whole process result in the emission of radiation and hence the discharge is termed as *glow discharge* [27]. Depending on the applied potential and the resulting discharge current, a plasma discharge can be divided into various regimes [27]. The process of sputtering, which is the prime focus of this work, belongs to the subdivision of the glow discharge which is called *abnormal glow*. In this

regime, the discharge voltage and current density increase with increasing the discharge power until the ion bombardment covers the whole surface of the target. Increasing the power further leads to the *arc discharge* regime, which is characterized by an extremely high current density at the target surface which in turn gives rise to plasma density in the order of 10^{21} m^{-3} [28].

As described earlier, a plasma is considered as quasi-neutral however, this attribute is mainly associated with the bulk of the plasma — as is the case with most of the plasma properties. Some deviations such as charge imbalance may occur at the plasma boundaries where the plasma interacts with other surfaces, such as the chamber walls. This is due to the fact that the electrons being lighter are more mobile than ions and therefore diffuse faster to the walls thereby leaving the bulk plasma at a higher potential (which is called plasma potential) as compared to the grounded chamber walls. Typically, the plasma potential is a couple of volts [24]. In addition, any other isolated electrode immersed in the plasma will be at slightly negative potential (floating potential) as compared to the ground, which is also an effect of the faster electrons. Overall, this means that at the interface where the plasma interacts with any other surface, there is a region where ions will outnumber the electrons. This region is called plasma sheath [28]. A plasma sheath is therefore a non-neutral region in contrast to the bulk of the plasma. The potential profile of a continuous plasma discharge indicating the plasma sheaths is depicted in Figure 5.

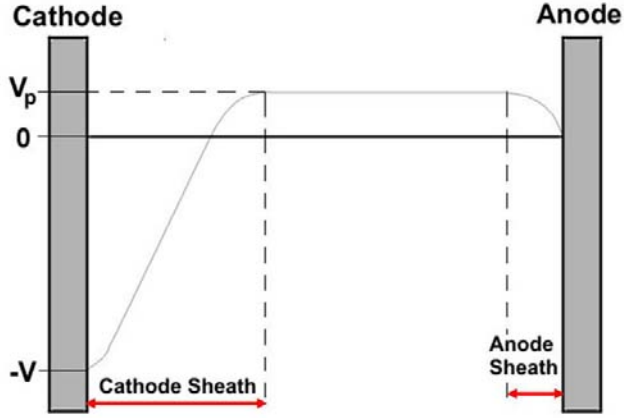


Figure 5. An schematic representation of the cathode and anode sheaths in a DC plasma discharge. The cathode represents the magnetron which is biased with potential $-V$ and the anode represents the chamber walls whereas V_p is the plasma potential. (After M. Ohring [24].)

The sheath thickness is expressed in terms of a characteristic plasma parameter which is called the Debye length, λ_{D_e} , and it is given as [24],

$$\lambda_{D_e} = \left(\frac{\epsilon_0 T_e}{en_0} \right)^{1/2} . \quad (3.3)$$

Here ϵ_0 is the electric permittivity constant, T_e is the electron temperature, e is the elementary charge and n_0 is the plasma density under the equilibrium condition ($n_i = n_e = n_0$). The Debye length is the length scale over which a significant departure from charge neutrality can be maintained [24].

It has been discussed earlier that in low-temperature gas discharge plasmas T_e is higher than the ions and neutral atoms temperatures (here denoted as T_i and T_g respectively). The electron energy distribution function (EEDF) in such a plasma discharge is non-Maxwellian (often bi-Maxwellian) [24]. This means that the EEDF consists of two electron populations, a low-energy population (called cold electron population) and a high-energy population (called hot electron population). Usually the average

temperatures of the cold and hot electron populations, denoted as $T_{e_{cold}}$ and $T_{e_{hot}}$ respectively, are used as the representative and characteristic parameters for the respective populations. An example of such an EEDF from the measurements performed in a C-HiPIMS discharge in this work is presented in Figure 6.

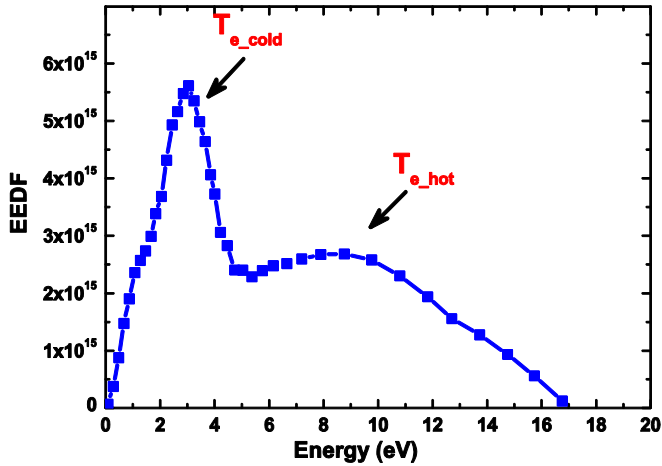


Figure 6. An EEDF from a Ne-HiPIMS discharge of carbon, showing two distinct electron populations (cold and hot).

3.3 Ionization Processes

Electron temperature, T_e , along with plasma density, n_e , is the most influencing parameter in establishing how the plasma constituents interact with each other. In the plasma chemistry many mechanisms are working in parallel, which means that these two parameters are also important in determining dominating reactions through which the ionization of the sputtered material occurs. In a sputtering plasma, the most common ionizing mechanisms for sputtered material are, direct electron impact ionization, electron impact ionization of excited sputtered atoms and the ionization via the interaction with excited sputtering gas atoms (also called Penning ionization). These mechanisms are respectively represented as [26],





where M and G respectively represent the sputtered and sputtering gas atoms.

Plasma discharges with high values of n_e are dominated by electron impact ionization (processes in equations (3.4) and (3.5)) while the low n_e discharges are dominated by Penning ionization (process in equation (3.6)) [29]. This is demonstrated in Figure 7 for the sputtering discharge of Al using Ar [29].

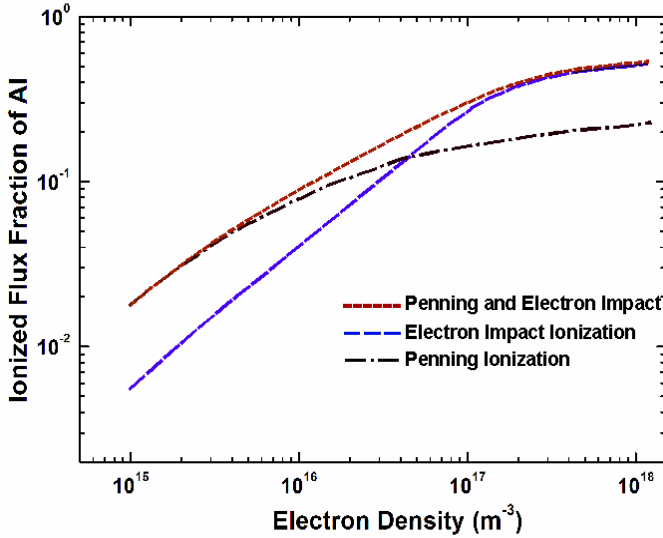


Figure 7. The process of ionization of sputtered Al at 36 mTorr of Ar gas pressure showing the region of dominance for electron impact and Penning ionization processes. (After J. Hopwood [29].)

Figure 7 also demonstrates that a higher ionized fraction for the sputtered material is obtained with increased n_e . This is a general trend for the sputtered material however, the absolute number of the ionized fraction varies with the material dependent cross sections for ionizing reactions. Metals are readily ionized with n_e in the range of 10^{16} to 10^{19} m^{-3} while the ionized fraction for non-metals such as carbon is low in this plasma density region [26]. One of the factors for the low ionized fraction for the case of non-metals is their higher ionization energies (here denoted as E_i) as compared to metals (for example,

E_i for C is 11.26 eV while for Al it is 5.98 eV). The dependence of the ionized fraction of the sputtered material on the plasma density is demonstrated in Figure 8 for various materials [26].

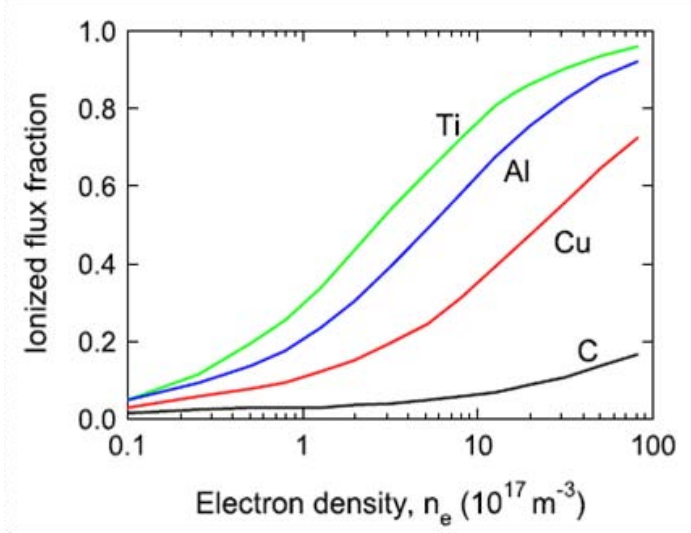


Figure 8. The ionized flux fraction dependence on plasma density for different materials. (After J. Hopwood [26].)

The dependence of the degree of ionization of the sputtered material on T_e and n_e can also be understood by looking at the mean ionization length of a sputtered atom, which is the average distance the sputtered atom travels before it is ionized in a plasma discharge [26]. For the electron impact ionization, the mean ionization length (here denoted as λ_{miz}) of the sputtered atom can be expressed as [26],

$$\lambda_{miz} = v_s / (k_{miz} n_e), \quad (3.7)$$

where v_s is the velocity of the sputtered atom and k_{miz} is the rate constant for electron impact ionization which is expressed as,

$$k_{miz}(T_e) = k_0 \exp(-E_0/T_e). \quad (3.8)$$

The constants E_0 and k_0 are material dependent and they can be extracted from experiments or computer simulations [26, 30,31].

Equation (3.7) shows that an increase in both, T_e and n_e will result in the decrease in the λ_{miz} which implies that the probability of the ionization of the sputtered material will increase. The exponential nature of k_{miz} (see equation (3.8)) suggests that the degree of ionization of the sputtered material is more sensitive to the changes in T_e as compared to n_e . As an example, the k_{miz} calculated using equation (3.8) for T_e from 1 eV to 5 eV and a constant value of n_e in a C-HiPIMS discharge is presented in Figure 9. It can be observed that a change of T_e from 1 eV to 5 eV increases the k_{miz} by about 4 orders of magnitude.

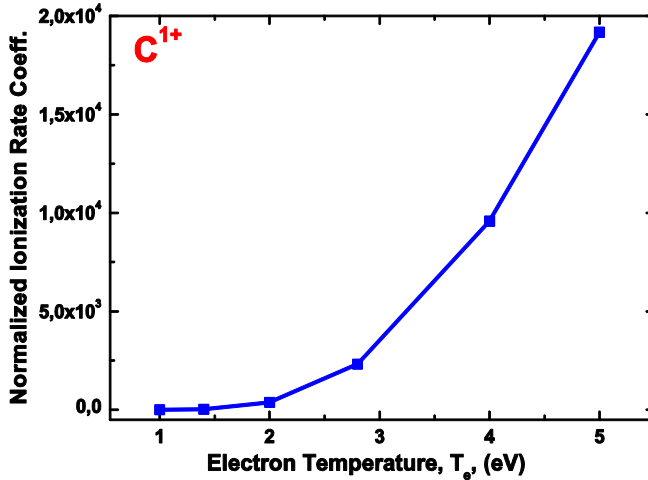


Figure 9. k_{miz} calculated for a C-HiPIMS discharge operated with a mixture of Ar and Ne sputtering gases. Increased values of T_e are obtained with an increase in the Ne content of the sputtering gas whereas the Ar content of the mixture is constant.

4. Amorphous Carbon Growth

4.1 Introduction

Amorphous carbon (a-C) can be grown in variety of different forms; from pure disordered structure to crystalline as well as in hydrogenated (often denoted as a-C:H) and hydrogen-free forms [4,5]. The versatility of the material stems from its different hybridization states i.e. sp^1 , sp^2 and sp^3 bond configurations, which are depicted in Figure 10 [5]. In sp^1 configuration, two of the four valence electrons of a carbon atom form σ (sigma) bonds directed along one plane (say x-plane) with its neighboring atoms, while the remaining two undergo a π (pi) bond formation in y and z planes. In sp^2 bond coordination, three of the four valence electrons form σ bonds with neighboring atoms in the plane while the fourth electron forms a π bond, which is perpendicular to the σ bond plane. This means that the interlayer bonding is based on weaker π bonds. In sp^3 configuration, all four valence electrons enter into σ bonds with neighboring atoms [5]. Since the σ bond is stronger as compared to π bond, the a-C film which are rich in sp^3 bonds exhibit higher hardness than the one which is rich in sp^2 bonds. In a-C:H, the sp^3 bonds are contributed by C-H sp^3 hybridization along with the C-C sp^3 hybridization.

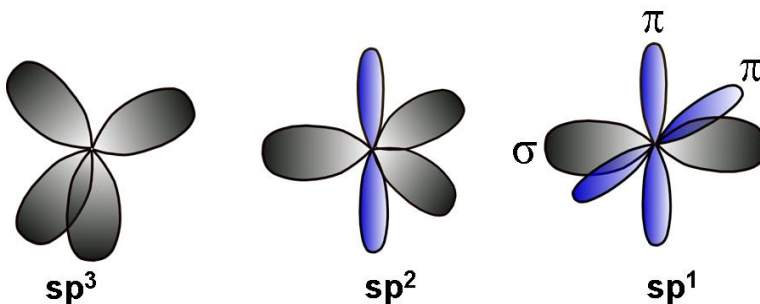


Figure 10. Illustration of sp^1 , sp^2 and sp^3 hybridizations of carbon. (After J. Robertson [5].)

4.2 Different Forms of Amorphous Carbon

Possible forms of a-C are represented by the ternary phase diagram of a-C growth in Figure 11 [5]. The bottom right corner on this diagram defines the region where no C-C atomic bonds exist and therefore, no film formation is possible. Adjacent to that is the region of hydrocarbons. The bottom left corner is the region of sp^2 rich carbon, examples of which are glassy carbon and pure graphite. Navigating along the left hand side, results in the bond fraction tailoring from sp^2 to sp^3 . With films containing ideally no hydrogen, an increase in the sp^3 bond fraction (about 50% or more) leads to the regime of diamond-like carbon (DLC). With further increase in the sp^3 bonds (about 75% or more), the films are referred to as tetrahedral a-C (ta-C). It is also possible to reach to the middle of the triangle if the a-C films contain high amount of hydrogen and at the same time, exhibit a very high density. This regime is called ta-C:H [5].

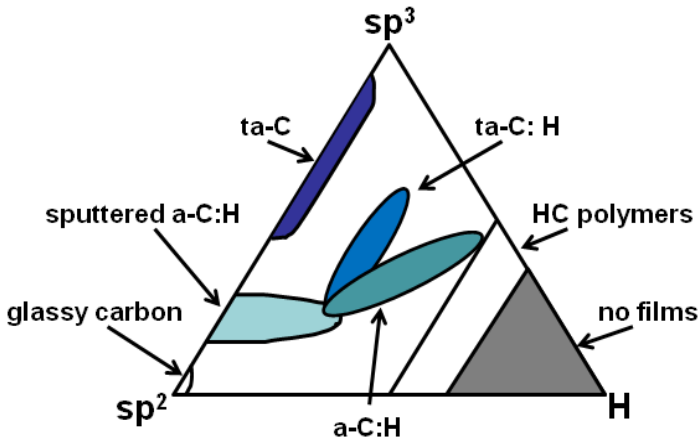


Figure 11. Ternary phase diagram for a-C growth. (After J. Robertson [26].)

4.3 The Densification Model

As discussed in chapter 1, the sp^3/sp^2 bond ratio is vital for the functionality of hydrogen free a-C, which is the prime subject of this thesis. The sp^3/sp^2 bond ratio can be tailored by controlling the flux and energy of the depositing species. For the a-C growth, the dependence of energy and flux of the depositing species is described by the densification model [5] which is illustrated in Figure 12.

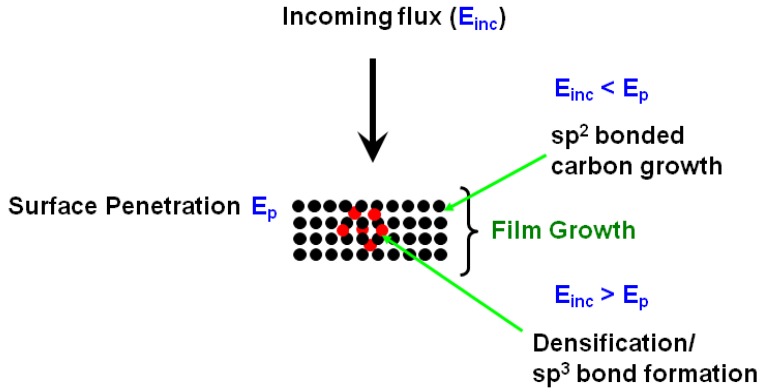


Figure 12. An schematic showing the densification model for the growth of a-C. (After J. Robertson [5].)

The densification model can be described as follows: Suppose that the depositing species possess a certain energy E_{inc} and the atoms at the surface of the growing film are bounded with an energy E_b . Associated with these surface atoms, there is an energy which is termed as displacement energy, E_d , which is the energy required to displace an atom and form a vacancy-interstitial pair. The surface penetration threshold, E_p , is the combination of E_d and E_b , such that [5],

$$E_p = E_d + (-E_b). \quad (4.1)$$

If E_{inc} is lower than E_p , the incoming atoms reside on the surface in lower energy configuration, resulting in the outward growing sp^2 layers. If E_{inc} is greater than E_p , the incoming atoms penetrate through the surface and shallow implantation (also referred to as subplantation) occurs. This results in the increase in the vacancy-interstitial pairs thereby causing an increase in the local density in the subsurface region. Since the material is amorphous therefore, the incident atoms and the implanted atoms are the same; a bond rearrangement from sp^2 to sp^3 occurs, which gives rise to an increase in the density of the films.

The process of implantation can occur in different ways. This depends on the energy of the incoming species. If E_{inc} is slightly higher than E_p , the direct penetration occurs. At

moderately higher incident energies as compared to E_p , the implantation occurs through the process of knock-on. At very high energies, thermal spike is caused. In the case of upper limit of energy for the knock-on process and in the region of thermal spike, there is an excess energy than what is required for the implantation. This excess energy appears in the form of heat (phonon) which causes a bond relaxation from sp^3 to sp^2 and as a consequence, the density of the film decreases to the initial level (before the implantation occurs). The E_p for carbon is about 35 eV while the optimum energy for the implantation is found to be about 100 eV. Typical energy range of interest is between 10 – 1000 eV. With this energy range, initially a transition from sp^2 dominated growth to sp^3 dominated growth occurs, and after the optimum is reached, the relaxation occurs. Figure 13 shows the experimental verification of the densification model including the processes of densification and relaxation [32].

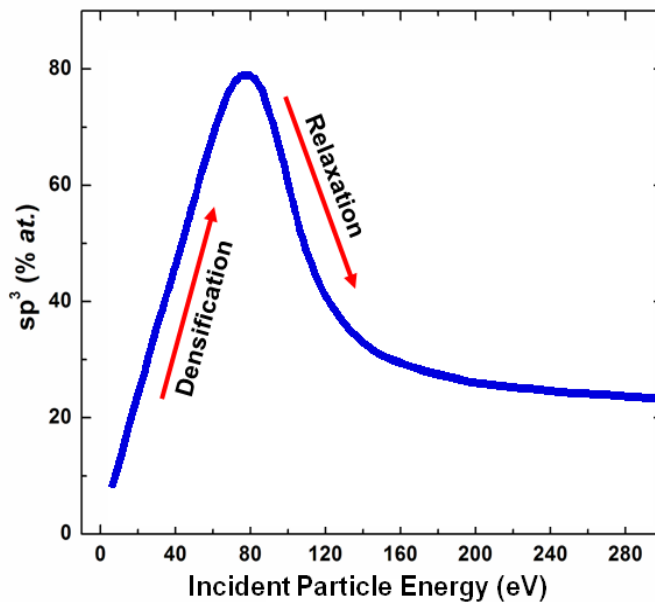


Figure 13. An experimental verification of the densification model of a-C growth showing the dependence of the densification and relaxation on the energy of the depositing ions. (After Mckenzie [32].)

From the discussion of the densification model, it can be understood that the growth of denser and sp^3 rich a-C requires an energetic depositing flux. It is also important that the energy of the depositing flux can be controlled. This will be much easier if a large

fraction of the depositing flux is ionized. Highly ionized depositing fluxes are provided by the IPVD methods therefore, it is instructive to discuss the role of IPVD methods for the growth of a-C films.

5. Amorphous Carbon Growth and Ionized PVD

Among the IPVD methods, the state of the art approaches for the growth of denser and sp^3 rich a-C include FCVA and PLD. HiPIMS has successfully demonstrated its potential as an IPVD method for most commonly used metals (such as Cu, Ti, Ta). It is therefore also important to discuss the role of HiPIMS for the growth of a-C. In the following sections, a brief account of each of these methods will be presented in connection to the growth of a-C.

5.1 Filtered Cathodic Vacuum Arc

Cathodic vacuum arc discharges are the forefront of ion-assisted energetic deposition. In a cathodic arc discharge, the source material is vaporized by using a high-current, low-voltage arc at the target (cathode) surface [17]. The arc forms cathode spots which are non-stationary locations of current density in the range of $10^6 - 10^8 \text{ Acm}^{-2}$. The associated power density is in the order of 10^7 Wcm^{-2} . Such a high current and power densities result in the phase transformation of the target material — from solid to highly ionized plasma. The plasma thus generated expands into vacuum ambient, with its constituting ions possessing a velocity in the order of $1 - 2 \times 10^4 \text{ ms}^{-1}$, resulting in the ion energies between 20 eV to 200 eV while the ionized fraction of the source material can reach up to 100% [17]. Creation of highly ionized depositing fluxes in such a discharge is also accompanied by the ejection of droplets and debris particles from the cathode surface — commonly known as macroparticles. The size range of the macroparticles is in the order of $0.1 - 100 \text{ }\mu\text{m}$. These particles are incorporated into growing films and deteriorate the film quality. There are various methods which are employed to filter the

macroparticles out before they reach to the substrate. This filtration leads to the modified form of cathodic arc deposition, which is known as filtered cathodic vacuum arc (FCVA) [33]. FCVA discharges can be operated in DC as well as in pulsed mode. In the DC mode, the current is in the range of 50 – 150 A while the pulsed discharges provide higher current in the order of about 1000A [33, 34].

Plasma properties in FCVA such as n_e in the order of $10^{20} - 10^{21} \text{ m}^{-3}$, T_e up to 10 eV and the highly ionized (up to 100%) depositing flux — having ion energies as high as 200 eV — make it a suitable choice for the ion-assisted film growth especially for the synthesis of sp^3 rich a-C [10]. FCVA has been extensively employed for the synthesis of high density and sp^3 rich a-C. In such a case, C ion energies of about 20 – 30 eV in DC arc discharges while a wider energy range of 20 – 140 eV in pulsed arc discharges have been reported [10]. The energetic depositing flux of C has been shown to provide a-C films with mass density reaching up to 3.2 gcm^{-3} , sp^3 fraction of about 88% and the hardness of about 90 GPa [10]. The grown a-C film properties from FCVA are promising however, the drawbacks with this technique such as lack of lateral film uniformity, reduction of the deposition rate due to macroparticle filtration as well as difficulty to produce defect-free coatings (due to the fact that 100% macroparticle filtration can not be achieved) are the major concerns over its implementation at industrial scale especially for the production of high quality and cost-effective a-C coatings for optical and electronic applications.

5.2 Pulsed Laser Deposition

In PLD, the source material is evaporated using laser irradiation in the form of small (15 – 30 ns) pulses. The process of evaporation is accompanied by a luminous intensity plasma cloud hurled over and traveling normal to the target, which is also called ‘plume’. The plume contains high-energy (substantially higher than thermal energies) neutrals and ionized atoms as well as clusters of the target material [16, 35]. Commonly used lasers for the process of pulsed laser deposition are 193 nm ArF and 248 nm KrF excimer lasers. In this method, the power densities at the target surface due to focused laser beams can reach in the order of $50 - 500 \text{ MWcm}^{-2}$ [35]. For the case of a-C growth, the energies of the evaporated material and the plasma density in the plume meet the energetic

deposition conditions, which are required for the synthesis of sp^3 rich a-C. The densities of a-C grown with PLD as high as about 3 gcm^{-3} , with hardness of the films reaching 100 GPa have been reported [5,16,35] and therefore, the technique is regarded as a viable IPVD method for the synthesis of DLC and ta-C. However, there are drawbacks that are inherent to the method such as, source material cluster evaporation, lower deposition rate, costly setup, lack of lateral uniformity of the grown films as well as difficulty in making large area depositions [16]. These constraints limit the up-scaling of the technique and hence the irrelevance to the industrial setup results.

5.3 High Power Impulse Magnetron Sputtering

As it was discussed in chapter 2, a HiPIMS discharge is usually operated at the peak target power densities in the order of kWcm^{-2} , which results in n_e in the order of 10^{18} to 10^{19} m^{-3} [15]. The energy distribution of the sputtered material in a HiPIMS discharge follows a Thomson-like (Thomson distribution with high-energy tail) distribution. At low operating pressures, the high-energy tail may extend from 10 – 100 eV for the case of metals (such as for Ti) [18,19]. However, the low-energy thermalized ions still dominate the energy distribution, giving the average ion energy slightly higher than that of DCMS while the T_e is quite similar (few eV) to what is obtained from DCMS discharges [15]. This implies that the energetic deposition conditions do not exist unless the energy of the depositing flux is manipulated by some external means such as by applying a substrate bias potential. However, in contrast to DCMS, this is possible with HiPIMS as the ion-to-neutral ratio, due to 2 to 3 orders of magnitude higher n_e , is very high (up to 90% for Ti) [19].

The main reason for a highly ionized metal depositing flux achieved in the case of a HiPIMS discharge is the low E_i values of metals (which are typically in the range of 6 to 8 eV for commonly used metals). Non-metals such as carbon, on the other hand, have substantially higher E_i values (such as 11.26 eV for C) and therefore, they are difficult to ionize even with HiPIMS. For the case of carbon, the C^+/C^0 ratio not exceeding 5% has been reported so far using HiPIMS [20]. This means that the electron impact ionization cross section for C is low as well as the electrons do not have sufficient energy to ionize

C despite the fact that the plasma density is high. Highly ionized depositing fluxes of sputtered carbon are therefore not achieved, which are essential for the synthesis of denser and sp^3 rich a-C. The best results reported so far give the film density of about 2.2 gcm^{-3} and sp^3 bond fraction of about 45% using HiPIMS [21].

The state-of-the art of a-C growth emphasizes on the fact that in terms of film density and sp^3 bond fraction, the best results are obtained with FCVA and PLD. The quality of the coatings, the simplicity of the method and its cost effectiveness for large scale production as well as upscalability are desired for an industrial process and FCVA and PLD lack in these areas. HiPIMS, being a magnetron sputtering based technique, has a potential to demonstrate these features and therefore it can provide an industrially relevant process for a-C growth. In terms of film properties such as mass density and hardness, HiPIMS is well behind FCVA and PLD. The conventional HiPIMS process therefore requires modifications in order to produce a-C coatings with properties comparable to FCVA and PLD.

6. Research Strategy and Experimental Details

6.1 Research Strategy

It was discussed in the previous chapter that the difficulty encountered with HiPIMS in creating highly ionized C fluxes is mainly due to low electron impact ionization cross section for C and insufficient electron temperature, T_e . It should be noted that the plasma density, n_e , in C-HiPIMS discharge, comparable to that of metal-HiPIMS discharge (of the order of 10^{18} m^{-3} , as determined in this research) can be obtained. Thus, the only way to further increase the degree of C ionization in a HiPIMS discharge is by increasing T_e as show in equation (3.7). The strategy adopted in this research is based on increasing the ionization of C by increasing T_e in a C-HiPIMS discharge. The T_e of a plasma discharge is set by the ionization energy, E_i , of the sputtering gas. This implies that a plasma discharge created using a high E_i gas should contain energetic electrons. Conventional C-HiPIMS discharges are operated using Ar (E_i value of 15.6 eV) as sputtering gas. This means that higher T_e can be obtained if Ne or He (having E_i values of 21.56 eV and 24.58 eV respectively) is used, instead of Ar. In this work, Ne was used for C sputtering using a HiPIMS process at 2 Pa and 4.66 Pa. A difficulty encountered with Ne was its ignition at lower operating pressures, such as at 2 Pa, due to its high E_i value. This difficulty can be overcome by means of pre-igniting the discharge. In this work, a new method for the pre-ignition of a discharge is introduced, which uses a mixture of a low E_i gas (which is relatively easily ionized, such as Ar) and a high E_i gas (such as Ne in this case). This method was used for the experiments performed at lower pressure of 2 Pa. At this

pressure, a mixture of Ar and Ne from 0% Ne to 83% Ne was used (here 0% Ne condition corresponds to pure Ar). At higher pressure of 4.66 Pa, pure Ne discharge was used. The Ne-HiPIMS discharges were compared with pure Ar-HiPIMS discharges operated at both, 2 Pa and 4.66 Pa. The plasma parameters in the discharges (such as n_e and T_e) were determined by performing Langmuir probe measurements. The ionized fluxes of C and the energy distributions of C ions were measured by mass spectrometry. The mass densities of the resulting C films were determined by x-ray reflectometry. The results obtained from the plasma and film characterization are summarized in **paper I**.

The strategy for growing thin films on complex-shaped surfaces is based on using the dual-magnetron approach in an open-field configuration. In this approach, two circular unbalanced magnetrons, employing Ti targets and having the similar magnetic field configuration, are placed facing each other co-axially. The similar magnetic field configurations of the magnetrons results in opening up of the field lines sideways. This enhances the sideways transport of the sputtered Ti, which is subsequently deposited on the substrates placed perpendicular to the surface of the magnetrons. The magnetrons were operated synchronously using DCMS and HiPIMS under the identical process conditions. The comparison with a DCMS discharge was made for gaining an insight into the effects of the degree of ionization on the sideways transport of the sputtered flux. The process was optimized by varying the separation distance between the magnetrons as well as by varying the working gas pressure. The degree of ionization of the sputtered Ti was investigated by measuring the emission from the plasma discharges using optical emission spectroscopy as well as by measuring the plasma parameters (such as n_e and T_e) by performing Langmuir probe measurement. The deposition rates and the microstructure of the grown films were investigated by scanning electron microscopy. The results obtained from the plasma and film characterization are summarized in **paper II**.

6.2 Plasma Characterization

The plasma characterization in the first part of the research work involved the determination of the plasma parameters (such as n_e and T_e) and the measurement of the

C^{1+} ion fluxes by measuring the C^{1+} ion energy distribution function (IEDF). The plasma parameters were determined by Langmuir probe measurements while the C^{1+} IEDFs were measured by mass spectrometry. In the second part, the plasma characterization involved the determination of n_e and T_e which was performed by Langmuir probe measurements and the ionized flux fraction of the sputtered Ti which was estimated by the optical emission spectroscopy. The details of the characterization tools and the measurements are presented in the following sections.

6.2.1 Langmuir Probe Measurements

The idea behind the Langmuir probe measurements is to collect current-voltage (I - V) characteristic of a plasma discharge using a probe (typically a cylindrical metal wire) to characterize the plasma. The method provides a possibility of determining important plasma parameters such as n_e and T_e by determining the electron energy distribution function (EEDF). The concept of plasma diagnosis by means of measuring the I - V characteristic using such a probe was introduced by Irving Langmuir in 1926 [24]. These probes are therefore called Langmuir probes.

In principle, any electrode immersed into a plasma which can draw ion and electron currents such as by applying external bias potential, can serve the purpose. The dimensions and the choice of the material of the probe are important since the probe is immersed into the plasma where it may subject to drawing large currents. Therefore, a high melting point material is chosen for the probe. The dimensions of the probe are chosen such that it may not affect the ionization and energy balance and discharge current distribution in the surrounding plasma. In this work, a cylindrical wire made of tungsten encapsulated in a ceramic insulating tube is used as a probe (the details will follow later in the section). The dimension of the probe is chosen according to the criteria [36] that the length of the probe should be greater than the radius of the probe tip as well as the radius of the insulating tube (to avoid shadowing effects) and these two radii should be greater than the Debye length (see equation (3.1) in chapter 3 for the Debye length).

A typical I - V characteristic of a plasma discharge is shown in Figure 14. V_f is the floating potential, which is the potential at which the ion and electron currents are equal and at this potential, a probe placed in the plasma does not draw any current. V_p is the plasma potential which is the potential of the plasma with respect to the grounded chamber walls. Usually, the plasma is at a positive potential (a couple of volts) with respect to the chamber walls which stems from a faster diffusion of the electrons through the chamber walls as compared to the heavier ions, leaving the plasma at a positive potential. The bias voltage (here denoted as V_b) can be regarded as positive or negative with respect to V_p . At $V_b = V_p$, the main contribution to the current is from electrons. For $V_b > V_p$, the probe is positive with respect to the plasma and the electron collection further increases reaching to the region of electron saturation. For $V_b < V_p$, the probe is negative with respect to the plasma and ion collection increases until V_b reaches to V_f . At this value, the probe does not draw any current ($I_{electron} = I_{ion}$). Decreasing V_b further, leads to the region of ion saturation. The ion saturation current is substantially lower than the electron saturation due to the much greater ion mass.

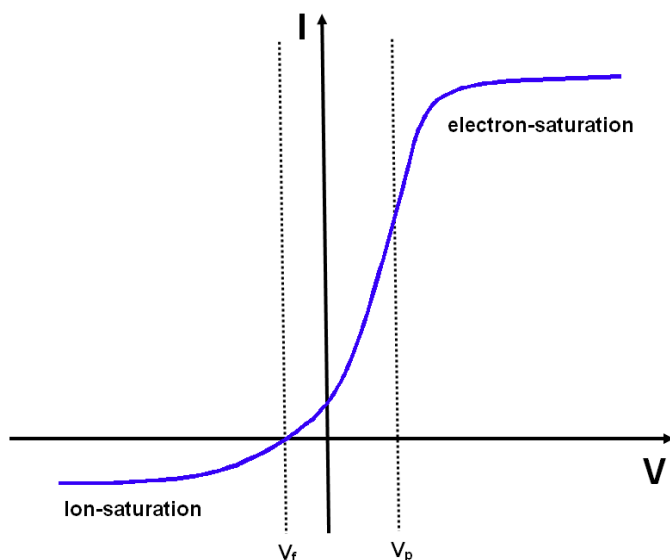


Figure 14. A typical I - V characteristic of a plasma discharge, obtained from Langmuir probe measurement. (After Lieberman [24].)

From the I - V characteristic of the plasma, EEDF is obtained using the Druyvesteyn formula [24],

$$g_e(V) = \frac{2m}{e^2 A_{pr}} \left(\frac{2eV}{m} \right)^{\frac{1}{2}} \frac{d^2 I_e}{dV^2}, \quad (6.1)$$

where A_{pr} is the probe area, m and e are the electron mass and charge, I_e is the electron current, and $V = V_p - V_B$ is the probe potential with respect to the plasma potential. Once the EEDF is known, the electron density is found by,

$$n_e = \int_0^{\infty} g_e(E) dE. \quad (6.2)$$

In low-pressure, weakly-ionized discharges, the EEDF is generally non-Maxwellian (often bi-Maxwellian) and the electron temperature is considered as an effective electron temperature, T_{eff} , representing the mean electron energy $\langle E \rangle$ determined from the EEDF. The average electron energy is,

$$\langle E \rangle = 1/n_e \int_0^{\infty} E g_e(E) dE, \quad (6.3)$$

and the effective electron temperature is defined as,

$$T_{eff} = 2/3 \langle E \rangle. \quad (6.4)$$

For the Langmuir probe measurements performed in this work, a cylindrical shaped Langmuir probe made of a thin tungsten wire having a length of 5 mm and a diameter of 125 μm was used. The probe was encapsulated into a ceramic insulating tube. The tip of the probe was immersed into plasma while the rear end of the probe was connected to the external circuitry for applying the bias voltage and measuring the resulting current drawn by the probe from the plasma body. For the Langmuir probe measurements performed in

the work presented in **paper I**, the probe was placed at the axis of the magnetron at a separation of 6 cm from the target surface while for the work presented in **paper II**, the probe was placed at the centre position between the two magnetrons. In both of the cases, the probe was lengthwise parallel to the target surface. The probe was biased with the help of a probe bias power supply. The bias voltage was varied with the help of a potential divider and the resulting probe current was measured as a voltage drop across a 1.1 Ohm shunt resistance. An analog-to-digital converter (PICO ADC 212 oscilloscope, 12-bit resolution module), triggered by the cathode pulse, was used in order to convert the analog form of the current/voltage into digital form to feed it to the computer. The data acquisition was performed by a lab-view program.

The probe bias voltage V_b was varied in steps of 0.02 volts, ranging from -40 Volts to +20 Volts, to collect the ion and electron currents. The measurements were made time-resolved for the case of HiPIMS, in order to take the temporal behavior of the discharge current into account. At each voltage step, the current was recorded in 500 equal time intervals, each having a width of 320 ns. This means that the current was recorded for 160 μ s after the initiation of the pulse. In this way, the I - V curve for each time value can be reconstructed and analyzed. Smoothing and filtering of the acquired data was performed for the purpose of noise suppression. This is necessary since the plasma itself is inherently noisy. Also, the EEDF is determined by using the second derivative of the I - V curve (see equation (6.1)) therefore, any noise present in the data can be greatly amplified during the differentiation. The noise suppression was performed by digital smoothing of the measured I - V characteristic curve by taking an average of 30 samples followed by Blackman window filtration. The details of how the digital smoothing and filtering works, can be found elsewhere [37].

6.2.2 Mass Spectrometry

The ionized flux of the sputtered carbon was measured using a mass spectrometer for Ne- and Ar-HiPIMS discharges and the results are presented in **paper I**. The mass spectrometer used, is capable of performing mass-selected, energy-resolved measurements in both, the time-averaged as well as in time-resolved modes. The plasma

species with energies up to 100 eV with a resolution of 0.05 eV and masses up to 500 amu with a resolution of 0.01 amu can be recorded. The details of how the instrument performs a measurement, is briefly described as follows:

The mass spectrometer consists of electrostatic lenses, energy and mass filters and a detector, as shown in Figure 15. The operation of the spectrometer can be divided into four major sections which include, an extractor probe, energy filter, mass filter and a detector. The extractor probe includes a front end with an orifice, which is simply a circular entrance slit, of diameter between 50 μm to 300 μm , and an ionization source which is a filament which when heated through current, releases electrons. The ionization source is used when neutral species are analyzed such as during residual gas analysis (RGA). For the measurements of energy distribution functions of ions, the ionization source is turned off.

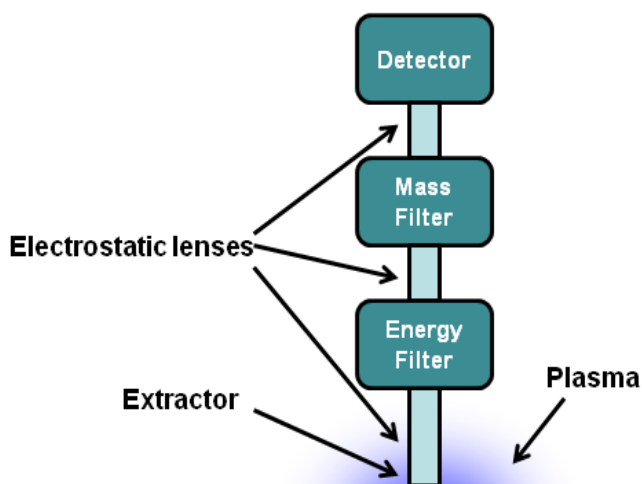


Figure 15. An schematic showing the main sections of a mass spectrometer.

The extractor probe is immersed into the plasma body with its front end biased, grounded or kept at a floating potential. The ions from the plasma are accelerated to the entrance slit with a potential difference, which is the difference between the plasma potential and the potential at the front end. The ions are then extracted and are focused to the entrance

of the energy filter using an electrostatic lens in the extractor section. The energy filter is a so-called Bessel box [38] which filters out the ions according to the selected energy. Ions of certain energy exit from the Bessel box which are again focused using an electrostatic lens to the mass filter. The mass filter is a quadruple mass filter which then filters out the ions of undesired mass and sends the species of the selected mass to the detector. The detector is the secondary electron multiplier (SEM) detector. The details of the Bessel box and the quadruple mass filter can be found elsewhere [38,39].

The ionized flux of the sputtered carbon was measured by recording time-averaged, energy-resolved IEDF for C^{1+} ions. The data was recorded for 100 ms using an energy range of 50 eV and the step size of 0.05 eV for both, Ne and Ar discharges operating with a pulse period of 1.66 ms (pulse frequency used was 600 Hz). In this way, C^{1+} IEDFs averaged over about 60 pulses were recorded at each energy step. The total ionized C^{1+} flux was calculated by integrating the C^{1+} ions over energy. A representative measured IEDF of C^{1+} ion is shown in Figure 16.

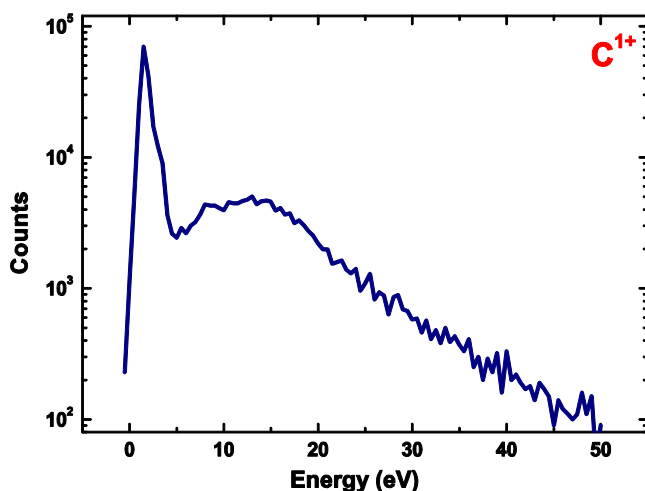


Figure 16. The C^{1+} IEDF measured for the case of 83% Ne discharge.

6.2.3 Optical Emission Spectroscopy

The qualitative information about the ionized fraction of the sputtered Ti and the sputtering gas (Ar in this case), during the sideways depositions of thin films, was

obtained by using optical emission spectroscopy (OES). In an OES measurement of a plasma discharge, the light emitted due to de-excitation of the plasma species (neutrals and ions), that are excited by collisions with energetic electrons, is collected. The collected emission is resolved into wavelength components and a spectrum is obtained [40]. OES is a simple and quick approach of gaining the qualitative information about the ionized fraction however, the quantification is difficult. This is due to the fact that the emission intensity does not only depend on the density of the emitting particles in the ground state, it is also affected by several other factors such as re-absorption of the emitted radiation, electron temperature and density as well as the electron-impact excitation cross sections [40].

The operation of an OES setup can be described as follows: The optical emission from a plasma discharge is collimated and subsequently directed to a slit. The grating and mirror arrangement resolves the component wavelengths of the collected emission. The spectrum thus obtained is sent to a photo-diode array or to a charged couple device (CCD) camera, which converts the optical signal into electrical signal. The electrical signal is thus sent to the processing unit. In this way, a spectrum containing the emission intensities plotted against the wavelength of the radiations from the plasma constituents is obtained.

In this research, a Mechelle Sencicam 900 spectrometer was used for performing OES measurements in the DCMS and HiPIMS discharges of the dual-magnetron open-field sputtering process using Ti. The spectrometer is equipped with a CCD camera capable of measuring the full spectrum (300 – 1100 nm) with a time resolution of 100 ns. The emission from the plasma was measured through a side window of the chamber. The collimator was made focused at the center position of the separation between both of the magnetrons. The data was collected at the working gas pressures of 5, 10 and 20 mTorr for various separation distances between the magnetrons (3, 4, 5 and 8 cm). An example of an OES collected spectrum is presented in Figure 17.

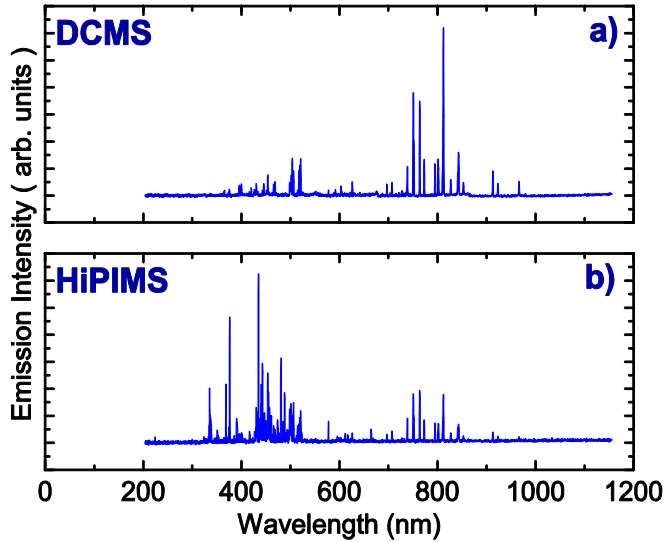


Figure 17. Optical emission spectra of a) Ti-DCMS discharge and b) a Ti-HiPIMS discharge obtained at 250 W of discharge power, at 10 mTorr of the working gas pressure and at 5 cm of the separation between the two magnetrons. The region in the spectra between 200 nm to 600 nm is dominated by Ti^0 and Ti^{1+} while the region above 600 nm is dominated by Ar^0 and Ar^{1+} .

6.3 Film Characterization

The film characterization in the first part of the research involved the determination of the mass density of the a-C films which was done by performing the x-ray reflectometric measurements on the films. In the second part, the film characterization involved the investigations on the microstructure of the grown Ti films, which were made by employing scanning electron microscopy. The details of the film characterization tools and the measurements are presented in the following sections.

6.3.1 Mass Density Measurements Using X-ray Reflectometry

X-ray reflectometry (XRR) is widely employed for the determination of mass density, surface roughness and film thickness of a-C films [10,41,42]. The method employs monochromatic x-rays to generate a characteristic pattern of a sample — which is an interference pattern, resulting due to the total external reflection of x-rays, as depicted in Figure 18 [44].

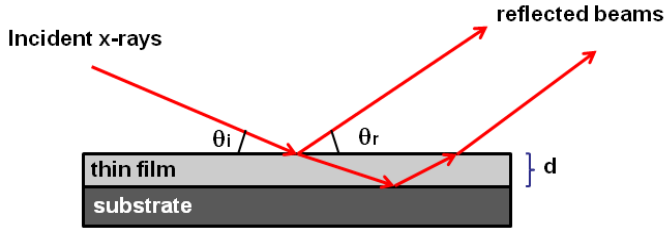


Figure 18. An schematic showing the principle of x-ray reflectivity.

Since the refractive index of x-rays is slightly less than unity, the total external reflection occurs at very small incidence angles. Due to this reason, grazing incidence angles are used and often, the method is also referred to as grazing incidence x-ray reflectometry. When the incidence angle increases above the critical angle (the angle at which total external reflection occurs), the x-rays start to penetrate into the film. The specular reflections from the air-film and from the film-substrate interfaces interfere to give the characteristic pattern. The critical angle, θ_c , for this case can be derived by using Snell's law at the air-film interface, which is expressed as [10,44],

$$\theta_c^2 = \frac{r_0 \lambda^2 Z N_A \rho_m}{\pi A} . \quad (6.5)$$

Here, r_0 is the classical electron radius, λ is the wavelength of x-ray radiation, Z and A are the charge number and mass number of the material, N_A is the Avagadro's number and ρ_m is the mass density of the material. By determining θ_c , the ρ_m of the sample can be determined using equation (6.5).

For the work presented in **paper I**, the XRR measurements were performed by using a Philips X'Pert-MRD diffractometer with de-coupled sample (ω) and detector (2θ) axes in reflection geometry. The diffractometer was equipped with a copper x-ray source (Cu, K_α $\lambda = 1.54 \text{ \AA}$) operated with 45 kV and 40 mA. In the primary path (between the x-ray source and the sample) a hybrid-mirror optics with a $1/32^0$ divergence slit and in the secondary path (between the sample and the detector) a triple-axis (for hybrid mirror)

monochromator was used. The data acquisition was performed by a proportional detector (PW1711/96) with 500 kcps maximum count rate. XRR measurements were performed by making ω - 2θ scans in such a way that the detector angle (2θ) was twice the incidence angle (ω) on the sample. The scans were made with 2θ range of $0^\circ - 1^\circ$ with the full-width at half maximum (FWHM) of 0.005° of the direct beam. An XRR curve resulting from such a measurement on one of the sample is shown in Figure 19.

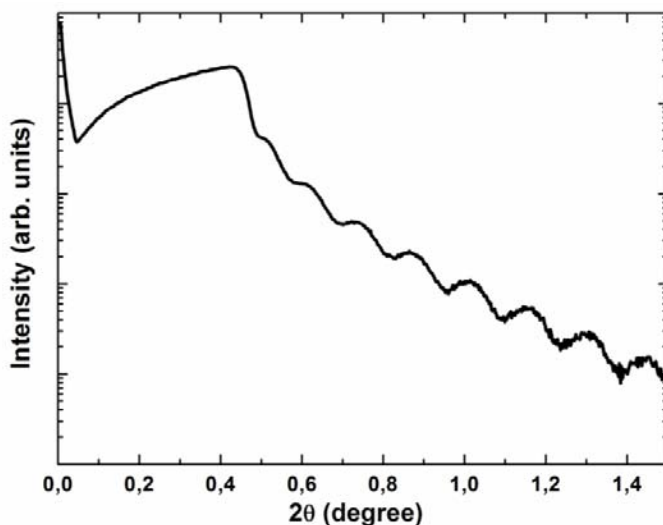


Figure 19. A characteristic XRR curve of an a-C film grown with 83% Ne discharge at -100 V of the substrate bias potential.

6.3.2 Scanning Electron Microscopy

Scanning electron microscopy (SEM) is widely used for collecting the surface topographic information of specimen by recording images. The images in an SEM are recorded by collecting the backscattered electrons and secondary electrons, which are emitted from the specimen in response to an incident electron beam [45] — which can be accelerated to the voltages up to 20 kV. For the work presented in **paper II**, the cross-sectional images of Ti films were obtained by a LEO 1550 Gemini SEM setup using an inLens detector. An acceleration voltage of 5 kV and magnifications of 35 kX and 50 kX were used. The results obtained from these measurements are summarized in **paper II**.

7. Summary

7.1 Paper I

In this paper, an alternate route for increasing the degree of ionization of carbon is introduced using a HiPIMS process. This alternate route is based on increasing the electron temperature, T_e , instead of increasing the plasma density, n_e . This is shown to achieve by using Ne for sputtering C in a HiPIMS discharge, instead of conventionally used Ar. The Ne-HiPIMS process provides higher T_e as compared to the Ar-HiPIMS process, whereas n_e and the process conditions in both of the discharges are identical. The fact that higher T_e in a plasma discharge results in an increase in the ionization of the sputtered material, is demonstrated by the use of the mean ionization length, λ_{miz} , (see equation (3.7)) which shows an order magnitude decrease when Ne is used. A good way to estimate the increase in C ionization is by measuring the ionized C fluxes, which was done by measuring the C^{1+} ion energy distributions using a mass spectrometer. At both, lower (2 Pa) and higher (4.66 Pa) operating pressures, use of Ne in the discharge provides more ionized C fluxes than Ar. At 2 Pa, the C^{1+} ion flux, with 83% Ne, is about 3 times higher than that obtained with pure Ar (0% Ne). A discharge with highly ionized C flux facilitates the growth of denser and sp^3 rich a-C films. This is demonstrated by growing the a-C films using Ne-HiPIMS and Ar-HiPIMS discharges. The mass densities of the grown films, measured by X-ray reflectometry, shows that in the case of Ne films with density as high as 2.8 gcm^{-3} can be grown — which is substantially higher than what has been obtained with conventional magnetron sputtering methods.

7.2 Paper II

In this paper, a new process for depositing films on complex-shaped substrates is developed. The new process uses the dual-magnetron approach in an open-field (magnetic field) configuration. The open magnetic field configuration enhances the sideways transport of the sputtered flux — an effect which was observed by Lundin *et al.* in a HiPIMS process [45]. The sideways deposition of thin films is demonstrated by operating the two magnetrons, which are equipped with Ti targets, synchronously using DCMS and HiPIMS under the identical process conditions. In order to optimize the growth rate, the separation between the magnetrons was varied from 3 to 8 cm. It was found that for both, the DCMS and HiPIMS discharges, the highest growth rate is obtained at a separation of 8 cm. The enhancement of the sideways transport depends on the ionized fraction of the sputtered flux therefore an estimate of the degree of ionization is made by characterizing the DCMS and HiPIMS discharges using optical emission spectroscopy (OES) as well as by performing Langmuir probe measurements. The OES measurements show that the HiPIMS discharge is dominated by the emission from Ti^{1+} and Ar^{1+} ions while the DCMS discharge is dominated mainly by the respective neutral species. Langmuir probe measurements show that the plasma densities in the order of 10^{18} m^{-3} and 10^{16} m^{-3} are obtained in the HiPIMS and DCMS discharges respectively. The growth rate, film uniformity and the plasma properties demonstrate a successful implementation of the dual-magnetron open-field approach for the sideways deposition of thin films — which is valuable for coating the complex-shaped surfaces.

8. Future Outlook

The results presented so far demonstrate that highly ionized C fluxes can be obtained by using Ne-based HiPIMS process, which facilitates the growth of high density a-C films. The further optimization of the process and future research will continue in the similar fashion i.e. new ways will be developed to enhance the plasma properties and the influence on the film properties will be investigated.

In one of the ongoing work, a detailed investigation on the film properties is performed which involves; the investigation on the mechanical properties of the films such as hardness, Young's modulus as well as the bonding properties of the films i.e. the sp^3 to sp^2 bond ratio are being investigated. The incorporation of the residual H and the sputtering gas species into the films are also investigated.

The a-C films containing high sp^3 bond fraction are known to suffer with residual stresses as well as with poor adhesion of the films to the substrate. The aim of one of the future study is to address these issues. The goal is to demonstrate the good adhesion of thicker (in the order of micron) and sp^3 rich a-C films on steel substrates.

The feasibility of sideways deposition of thin films using the dual-magnetron open-field approach has so far been demonstrated by using Ti. In the future study, the sideways deposition of a-C films will be performed by employing the newly developed Ne-based HiPIMS process. The conventional Ar-HiPIMS process will also be used to investigate the effect of the degree of ionization of the sputtered C on the sideways transport as well as on the microstructure of the depositing films.

9. References

- [1] M. Ohring, *Materials Science of Thin Films: Depositions & Structure 2nd Edition*, San Diego, USA: Academic Press, (2002).
- [2] M. Antler, Gold in electrical contacts, (1968).
- [3] M. Klaus, C. Genzel, *Advanced Engineering Materials* 13 (2011) 845-850.
- [4] C. A. Charitidis, *International Journal of Refractory Metals and Hard Materials* 28 (2010) 51-70.
- [5] J. Robertson, *Materials Science and Engineering: R: Reports* 37 (2002) 129-281.
- [6] U. Jansson, E. Lewin, M. Råsander, O. Eriksson, B. André, U. Wiklund, *Surface and Coatings Technology* 206 (2011) 583-590.
- [7] K. Baba, R. Hatada, S. Flege, W. Ensinger, *Advances in Materials Science and Engineering* 2012 (2012) 1-5.
- [8] N.M.J. Conway, a. C. Ferrari, a. J. Flewitt, J. Robertson, W.I. Milne, a. Tagliaferro, W. Beyer, *Diamond and Related Materials* 9 (2000) 765-770.
- [9] S. Logothetidis, M. Gioti, P. Patsalas, C. Charitidis, *Carbon* 37 (1999) 765-769.
- [10] A.C. Ferrari, A. Libassi, B.K. Tanner, V. Stolojan, J. Yuan, L.M. Brown, S.E. Rodil, B. Kleinsorge, 62 (2000) 89-103.
- [13] J. Bohlmark, M. Ostbye, M. Lattemann, H. Ljungcrantz, T. Rosell, U. Helmersson, *Thin Solid Films* 515 (2006) 1928-1931.
- [14] J. Alami, P.O. Å. Persson, D. Music, J.T. Gudmundsson, J. Bohlmark, U. Helmersson, *Journal of Vacuum Science & Technology A: Vacuum, Surfaces, and Films* 23 (2005) 278.
- [15] U. Helmersson, M. Lattemann, J. Bohlmark, A.P. Ehasarian, J.T. Gudmundsson, *Thin Solid Films* 513 (2006) 1-24.
- [16] R. Eason (Ed.), *Pulsed Laser Deposition of Thin Films: Applications-led Growth of Functional Materials*, Wiley (2006).

- [17] A. Anders, *Cathodic Arcs: From Fractal Spots to Energetic Condensation* Springer (2010).
- [18] K. Sarakinos, J. Alami, S. Konstantinidis, *Surface and Coatings Technology* 204 (2010) 1661-1684.
- [19] J. Bohlmark, J. Alami, C. Christou, A.P. Ehiasarian, U. Helmersson, *Journal of Vacuum Science & Technology A: Vacuum, Surfaces, and Films* 23 (2005) 18.
- [20] B.M. Dekoven, P.R. Ward, R.E. Weiss, S. Clara, D.J. Christie, R.A. Scholl, W.D. Sproul, F. Tomasel, A.E. Industries, F. Collins, A. Anders, L. Berkeley, (2003).
- [21] K. Sarakinos, a. Braun, C. Zilkens, S. Mráz, J.M. Schneider, H. Zoubos, P. Patsalas, *Surface and Coatings Technology* 206 (2012) 2706-2710.
- [22] P. Signumd, *Phys. Rev.* 184 (1969) 383.
- [23] D. M. Mattox, *Handbook of Physical Vapour Deposition (PVD) Processing: Film Formation, Adhesion, Surface Preparation & Contamination Control*, New Jersey, USA: Noyes Publications, (1998), pp. 472.
- [24] M.A. Lieberman and A.J. Lichtenberg, *Principles of Plasma Discharges and Materials Processing*, John Wiley & Sons, New York, USA (2005), pp. 39.
- [25] A. Bogaerts, E. Neyts, R. Gijbels, J. van der Mullen, *Spectrochimica Acta Part B: Atomic Spectroscopy* 57 (2002) 609-658.
- [26] J.A. Hopwood, in: J.A. Hopwood (ed), *Thin Films: Ionized Physical Vapour Deposition*, Academic Press, San Diego, (2000), pp. 181.
- [27] J. R. Roth, *Industrial Plasma Engineering Volume I: Principles*, Institute of Physics Publishing, Bristol, UK (1995).
- [28] A. Anders, *Surface and Coatings Technology* 183 (2004) 301-311.
- [29] J. Hopwood, F. Qian, *Journal of Applied Physics* 78 (1995) 758.
- [30] M.H. Lee and C.-W. Chung, *Phys. Plasmas* 12 (2005) 073501.
- [31] R.S. Freund, R.C. Wetzel, R.J. Shul, and T.R. Hayes, *Phys. Rev. A* 41 (1990) 3575.
- [32] D.R. McKenzie, D. Muller, B.A. Pailthorpe, *Phys. Rev. Lett.* 67 (1991) 773.
- [33] A. Anders, *Vacuum* 67 (2002) 673-686.
- [34] P.J. Martin, R.P. Netterfield, a. Bendavid, T.J. Kinder, *Surface and Coatings Technology*, 54-55 (1992) 136-142.
- [35] A. A. Voevodin, M.S. Donley, *Surface and Coatings Technology* 82 (1996) 199-213.

- [36] J.T. Gudmundsson, J. Alami, U. Helmersson, *Surface and Coatings Technology* 161 (2002) 249-256.
- [37] F. Magnus, J.T. Gudmundsson, *The Review of Scientific Instruments* 79 (2008) 073503.
- [38] J. Bohlmark, *Doctoral Thesis: Fundamentals of High Power Impulse Magnetron Sputtering*, Linköping University, Linköping, Sweden (2005).
- [39] P.E. Miller, M.B. Denton, *Journal of Chemical Education* 63 (1986) 617.
- [40] C. Christou, Z.H. Barber, *Journal of Vacuum Science & Technology A: Vacuum, Surfaces, and Films* 18 (2000) 2897.
- [41] Y. Hu, M. Chaker, J.N. Broughton, E. Gat, 85 (1994) 830-832.
- [42] M.F. Toney, S. Brennan, S. Synchrotron, 66 (1989) 1861-1863.
- [43] M. Birkholz, *Thin Film Analysis by X-ray scattering*, WILEY-VCH Verlag GmbH & Co. KGaA, Weinheim, Germany (2006).
- [44] J. Goldstein, *Scanning Electron Microscopy and X-ray Microanalysis*, 3rd Edition, Springer, New York, USA (2008).
- [45] D. Lundin, P. Larsson, E. Wallin, M. Lattemann, N. Brenning, U. Helmersson, *Plasma Sources Science and Technology* 17 (2008) 035021.